ACS EARTH AND SPACE CHEMISTRY

http://pubs.acs.org/journal/aesccq

Article

Effects of Oxyanion Surface Loading on the Rate and Pathway of Ferrihydrite Transformation

Alireza Namayandeh,* Olaf J. Borkiewicz, Nefeli M. Bompoti, Steven K. Watson, James D. Kubicki, Maria Chrysochoou, and F. Marc Michel

Cite This: https://doi.org/10.1021/acsearthspacechem.3c00232

Read Online

ACCESS | Metrics & More | Article Recommendations | Supporting Information

ABSTRACT: In natural environments, ferrihydrite (Fh) reacts readily with the contaminant and nutrient oxyanions through surface complexation. While previous experiments showed that the transformation of Fh to Gt and Hm under oxic conditions at 70 °C is controlled by the type and strength of oxyanion surface complexes, the impact of surface loading on this process is only partly understood. Synchrotron scattering methods and chemical analysis were used to develop a kinetic model that describes the impact of oxyanion surface loading on the rate and pathway of Fh transformation by using arsenate (AsO_4^{3-}) and phosphate (PO_4^{3-}). Kinetic modeling showed that AsO_4^{3-} and PO_4^{3-} adsorption decreased the rate of transformation and favored Hm formation over Gt. Higher surface loadings increasingly inhibited Fh transformation with a greater effect for PO_4^{3-} compared with AsO_4^{3-}. This information has implications for understanding the impacts of oxyanions on the transformation of natural Fe to Gt and Hm in environmental systems.

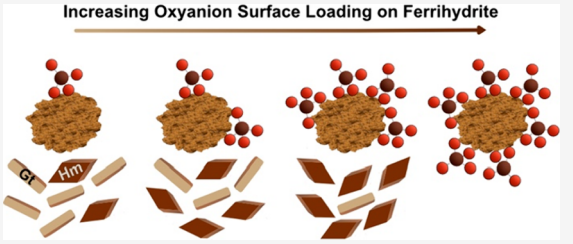

KEYWORDS: *hematite, goethite, arsenate, phosphate, hydration, oriented attachment, dissolution/recrystallization*

INTRODUCTION

Ferrihydrite (Fh) is a nanosized iron oxyhydroxide that immobilizes contaminants and nutrients such as metal and metalloid oxyanions in natural environments through surface complexation reactions.[1−14] Immobilization may be temporary as Fh ($Fe_{1.0}O_{0.67}(OH)_{1.63}$)[15] metastability causes it to eventually transform to larger crystalline products such as goethite (Gt; α-FeOOH) and hematite (Hm; α-Fe_2O_3).[16−31] Transformation and growth reduce the reactive surface area and change the type and availability of surface functional groups, resulting in the desorption of preadsorbed oxyanions to solution.[20,26,32,33] Elevated concentrations of oxyanions mobilized from mineral surfaces can cause severe environmental problems.[9,34] For instance, more than 100 million people worldwide are exposed to dissolved arsenic (e.g., arsenate; AsO_4^{3-}) concentrations in groundwater that exceed acceptable drinking water standards.[35−40] Although sulfate (SO_4^{2-}), phosphate (PO_4^{3-}), and nitrate (NO_3^-) are not regulated as being toxic, their excessive concentrations in aquatic environments from mining and agriculture activities are known to be detrimental, for example, eutrophication of surface water.[41−46]

In aqueous environments, oxyanion adsorption on the Fh surface is controlled by various factors, including pH, ionic strength (I), surface loading, type of adsorbent, competing ions, and time.[1,9,34,47−53] Arsenate and PO_4^{3-} show a high affinity for adsorption on the surface of iron oxy-hydroxides, particularly at acidic to intermediate pH.[3,12,52,54−57] Although intrinsic chemical differences, such as the smaller ionic radius of PO_4^{3-} and the redox sensitivity of AsO_4^{3-}, may result in their different biogeochemical behaviors under certain chemical conditions,[58] the chemical speciation of AsO_4^{3-} and PO_4^{3-} is analogous, and they are reported to compete for adsorption sites.[3,54−61] Prior studies have shown that AsO_4^{3-} and PO_4^{3-} dominantly form inner-sphere complexes on Fh under various chemical conditions. This is supported by a variety of experimental techniques such as attenuated total reflectance Fourier transform infrared spectroscopy (ATR-FTIR),[8,62] extended X-ray absorption fine structure (EXAFS),[57,63] differential pair distribution function (d-PDF) analysis,[64,65] and computational studies.[3,6] Bidentate complexes are usually the dominant type of surface species[12,53−57,60,66] although the fraction of monodentate complexes may increase with increasing AsO_4^{3-} and PO_4^{3-} surface loading in certain chemical conditions.[67]

The adsorption of AsO_4^{3-} and PO_4^{3-} on Fh through inner-sphere complexes reaches equilibrium either when all oxyanion molecules are adsorbed on the surface (i.e., low surface loading) or the entire available positive charges on the surface

Received: August 6, 2023
Revised: September 4, 2023
Accepted: September 12, 2023

are consumed by oxyanions (high surface loading).[67] In addition, oxyanion inner-sphere complexes remove hydroxyls and dehydrate the Fh surface, which steadily increases with increasing oxyanion surface loading.[1] Studies showed that the solvation effect, that is, the extent of dehydration of the adsorbing oxyanions, is much stronger for forming inner-sphere complexes than outer-sphere species,[68] and water is desorbed during inner-sphere reactions.[69,70] Therefore, the degree of hydration and positive charge controlled by inner-sphere complexes change with increasing oxyanion surface loading, which may impact the rate and pathway of Fh transformation. For example, some studies have reported that increasing AsO_4^{3-} surface loading on Fh at pH ∼ 10 and ∼1 °C inhibits the rates of both Fh transformation and Gt formation.[26,32] Others have reported that high AsO_4^{3-} and PO_4^{3-} surface loadings delay Fh transformation and favor Hm over Gt.[24] These studies have proposed that the adsorption of oxyanions controls the Fh transformation behavior. However, the mechanism of oxyanion adsorption on Fh through surface complexes is not identical for different oxyanions, and varied types of oxyanion surface complexes can have distinct effects on the rate and pathway of Fh transformation.[71] A more comprehensive study should account for the role of the oxyanion complex type and strength in controlling the rate and pathway of Fh transformation.

We recently developed a rate model that describes the effect of the oxyanion surface complex type and strength (i.e., weak electrostatic outer-sphere vs strong covalent inner-sphere) on the rate and pathway of Fh transformation.[71] We showed that NO_3^- outer-sphere complexes promoted the formation of Gt, whereas a mixture of outer-sphere and inner-sphere complexes for SO_4^{2-} induced the formation of Hm. Our previous work also showed that high surface loading (0.1 molar ratio) of AsO_4^{3-} inner-sphere complexes almost entirely suppressed the transformation of Fh, which made it impossible to thoroughly study the effects of AsO_4^{3-} inner-sphere complexes on the rate and pathway of Fh transformation. Therefore, the impact of AsO_4^{3-} inner-sphere complexes on the rate and pathway of Fh transformation is not well understood, which translates into limited predictive capabilities of Fh transformation and AsO_4^{3-} mobilization, particularly for lower AsO_4^{3-} surface loadings. Also, it was previously suggested that the degree of hydration on the Fh surface could potentially control the pathway of Fh transformation,[71] but no evidence was provided as to how oxyanions regulate the hydration on the Fh surface.

This work uses AsO_4^{3-} and PO_4^{3-} to evaluate the impact of oxyanion surface loading on the rate and pathway of Fh transformation under oxic conditions. Phosphate forms strong inner-sphere complexes on Fh,[3,8,57] similar to AsO_4^{3-}, which helps to confirm the impact of inner-sphere surface complexes. To the best of our knowledge, this is the first work to systematically quantify the rate of concurrent formation of Gt and Hm during Fh transformation in the presence of adsorbed AsO_4^{3-} and PO_4^{3-}. This information furthers our understanding of Fh transformation processes in natural and laboratory systems.

MATERIALS AND METHODS

Ferrihydrite Synthesis and Batch Adsorption. Two-line Fh was synthesized using a modified Schwertmann and Cornell protocol.[72] Specifically, 0.2 M Fe $(NO_3)_3$ was prepared and titrated to pH 7.5 ± 0.2 within 25 min by the addition of 2 M NaOH. The suspensions were centrifuged and dialyzed in an ultrapure (18.2 MΩ) water bath for several days until the conductivity of the water bath dropped below 20 $\mu S\ cm^{-1}$. Batch adsorption experiments were conducted in 50 mL centrifuge tubes using the Fh suspensions at a concentration of 5 g L^{-1}. For PO_4^{3-} (FhP) and AsO_4^{3-} (FhAs), four different concentrations (0.2, 0.6, 1.0, and 5.0 mM) of Na_2HAsO_4 and Na_2HPO_4 were prepared in a background of known $NaNO_3$ concentrations such that I was fixed at 0.1 M in all the samples. The AsO_4^{3-}/Fh and PO_4^{3-}/Fh molar (M) ratios of the adsorbed samples were ∼0.004 (FhAs_a and FhP_a), 0.012 (FhAs_b and FhP_b), 0.02 (FhAs_c and FhP_c), and 0.1 (FhAs_d and FhP_d). A set of Fh samples (control Fh) without oxyanions was prepared as a control. The pH of the samples was adjusted to 5.5 ± 0.2 using dropwise addition of 2 M NaOH. The samples were shaken inside an incubator at 25 °C for 24 h to allow the adsorption of oxyanions on Fh to reach equilibrium.[1,3,73] The samples were then centrifuged for 10 min at 7000 rcf to separate the supernatant from the solids. The supernatant was further centrifuged using a 0.22 μm centrifuge filter and analyzed by high-performance liquid chromatography − ion conductivity (IC) and inductively coupled plasma − optical emission spectroscopy (ICP-OES) to mass balance for the amount of oxyanion adsorbed on Fh. Visual MINTEQ was used to determine the concentration of the oxyanions used for different experiments (Table S1). All salts, acids, and bases were ACS reagent grade chemicals and used as received. No unexpected or unusually high safety hazards were encountered.

Fh synthesis, oxyanion adsorption, and transformation experiments were performed in air-equilibrated solutions. The concentration of dissolved inorganic carbon (DIC) in the solution at pH 5.5 ± 0.2 was calculated using Visual MINTEQ. Surface complexation modeling was utilized to estimate the amount of DIC adsorbed on Fh and predict the types of PO_4^{3-} and AsO_4^{3-} surface complexes. Also, the density functional theory (DFT) calculation was used to calculate dehydration on the Fh surface for AsO_4^{3-} and PO_4^{3-} adsorptions. Text S1 and Table S2 provide the details of the surface complexation modeling method and parameters. Text S2 gives details of the DFT method.

Transformation Experiment and Sample Treatment. The control and batch-adsorbed Fh samples were buffered using 0.4 M MES ($C_6H_{13}NO_4S$), and their pH was adjusted to 5.5 ± 0.2 using 0.1 M NaOH. Note that we added MES after the adsorption of AsO_4^{3-} and PO_4^{3-} reached equilibrium to avoid any competition between MES and oxyanions, although studies showed that MES only weakly bonds with the Fh surface.[74] They were then transferred to 10 mL of HDPE opaque plastic leak-proof bottles to perform the transformation experiment. The bottles were then placed in a sealed water bath in a mechanical convection laboratory oven (Thermo Scientific Heratherm) and aged at 70 ± 1.5 °C for 0, 24, 48, 72, 120, 168, 240, 360, 600, 888, and 1200 h. This temperature was selected to ensure the concurrent formation of Gt and Hm within a reasonable time scale for a laboratory experiment. Three replicates were prepared and aged at each time interval. The removed samples were centrifuged at 7000 rcf for 10 min. The collected pastes were air-dried for 24 h and powdered using a mortar and pestle.

Liquid and Solid Phase Characterization. The supernatants of the aged samples were analyzed using IC (PO_4^{3-}) and ICP-OES (AsO_4^{3-}) to determine the amounts of oxyanions desorbed during aging. Synchrotron high energy

https://doi.org/10.1021/acsearthspacechem.3c00232
ACS Earth Space Chem. XXXX, XXX, XXX−XXX

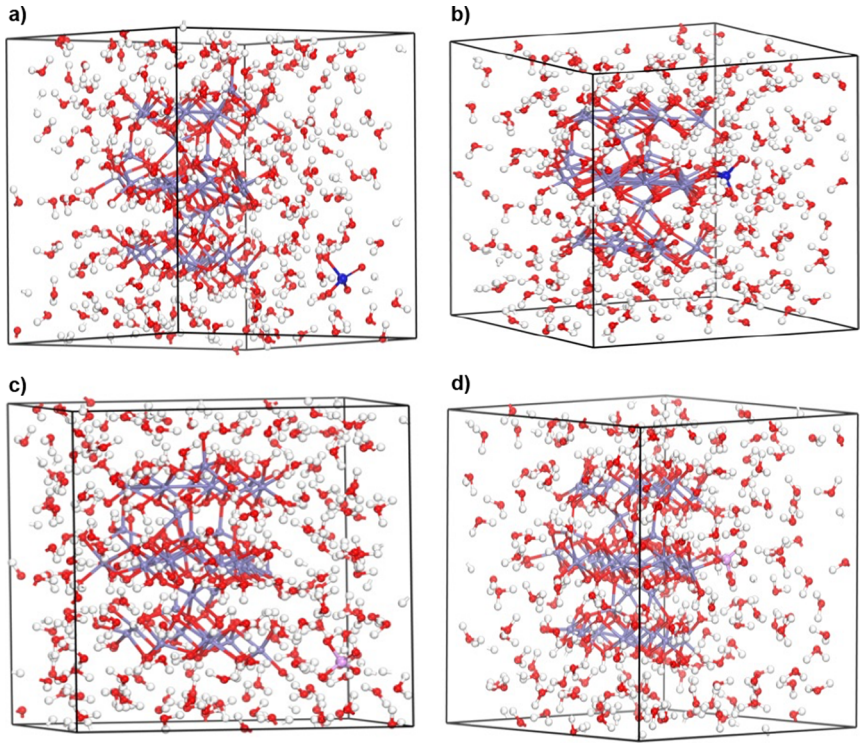

Figure 1. Structure of (a) AsO_4^{3-} in aqueous Fh, (b) AsO_4^{3-} inner-sphere complexation on Fh, (c) HPO_4^{2-} aqueous Fh, and (d) PO_4^{3-} inner-sphere complexation on Fh. H = white, O = red, Fe = blue-gray, As= blue, and *P* = purple.

X-ray scattering measurements were conducted at beamline 11-ID-B at the Advanced Photon Source, Argonne National Laboratory, to identify and quantify the solid phases. The raw scattering data were processed with GSAS-II by using established methods. xPDFsuite[75] was used to subtract the background and convert the data from reciprocal-space to real-space PDFs. The max Q-space for the Fourier transform was 24−25 1/Å. The phase abundances in the samples were quantified with linear combination fitting (LCF, WinXAS[76]) of the PDFs, using reference PDFs for synthetic 2-line Fh, Gt, and Hm. A kinetic model was developed to predict the transformation rate of control and adsorbed Fhs by using the obtained abundances of Fh, Gt, and Hm at each time point. The derived rate law is provided in Namayandeh et al.[71] and will be discussed in the following sections.

RESULTS AND DISCUSSION

Oxyanion Sorption Behavior. Surface complexation modeling showed that the adsorption of DIC on Fh was negligible, attributing to the significantly lower DIC/Fh molar ratio (0.0003) compared with that of oxyanions (Table S1). Results also showed that the bidentate complexes were the dominant type of bonding for both AsO_4^{3-} and PO_4^{3-} (>98%) adsorption, which is in agreement with previous experimental studies.[12,53−57,60,66] The concentration of the oxyanions in solution was measured both before and after aging. For FhAs and FhP samples, regardless of oxyanion concentration, AsO_4^{3-} and PO_4^{3-} were below the detection limits, showing that these oxyanions were completely adsorbed on the Fh surface and did not desorb significantly during aging. This is consistent with the surface complexation modeling results and reported high affinity of AsO_4^{3-} and PO_4^{3-} for adsorption on the surface of Fh and other iron oxy-hydroxides through strong complexes.[3,6−8,12,53,54,57,59,64,77−80]

The oxyanion inner-sphere complexes desorb water from the surface of Fh. The reactions for the adsorption of AsO_4^{3-} and PO_4^{3-} on Fh are as follows:

$$2{\equiv}FeOH + 2H^+ + AsO_4^{3-} \leftrightarrow ({\equiv}FeO)_2AsO_2^{2-} + 2H_2O$$

$$2{\equiv}FeOH + 2H^+ + PO_4^{3-} \leftrightarrow ({\equiv}FeO)_2PO_2^{2-} + 2H_2O$$

These reactions show that inner-sphere complexation occurs through ligand exchange that desorbs water, as modeled in a recent study using DFT.[81] The results confirmed the desorption of water during the adsorption of AsO_4^{3-} and PO_4^{3-}. Figure 1 shows the structures of the AsO_4^{3-} and PO_4^{3-} complexes. Also, the lists of bonds and H-bonds for both oxyanions are provided in Tables S3 and S4. The inner-sphere AsO_4^{3-} and HPO_4^{2-} replace two H_2Os that bonded with Fe. In addition, Fe−(OH)−Fe that is H-bonded to a H_2O molecule in $HAsO_4^{2-}$ and HPO_4^{2-} aqueous Fhs is H-bonded to an O in AsO_4^{3-} and HPO_4^{2-} after oxyanion adsorption, further decreasing water in the vicinity of the surface. This confirms previous studies[68−70] that reported the dehydration of the Fh surface during oxyanion inner-sphere complexation. Gu et al.[1] showed that oxyanion inner-sphere complexation on dry Fh was favored compared to outer-sphere complexation, suggesting that dehydration facilitates oxyanion inner-sphere complexation. They also reported that the ΔG of dehydration for oxyanions such as AsO_4^{3-} and PO_4^{3-} is insignificant during their adsorption on Fh, leading to their strong inner-sphere complexation on Fh.

Products and Pathway of Fh Transformation. The identities of the phases formed from the transformation of Fh with aging were determined by using synchrotron powder diffraction data. The peaks observed in samples that formed

https://doi.org/10.1021/acsearthspacechem.3c00232
ACS Earth Space Chem. XXXX, XXX, XXX−XXX

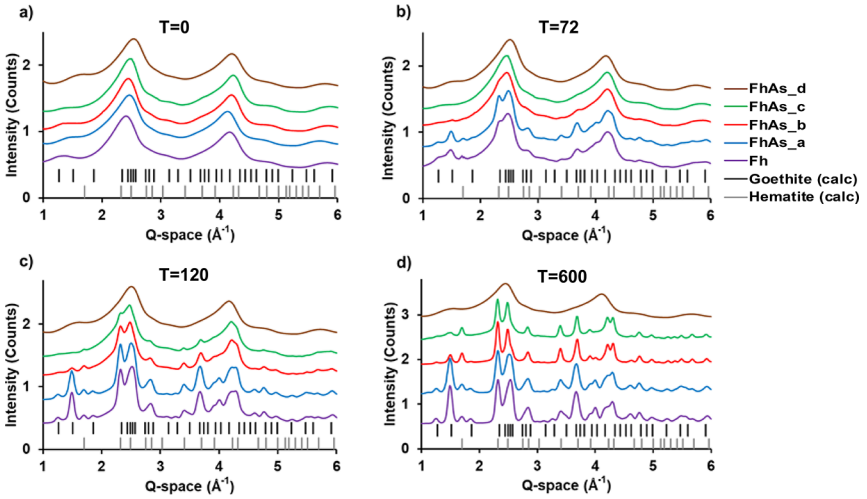

Figure 2. Synchrotron powder X-ray diffraction patterns for AsO_4^{3-}-adsorbed samples at (a) 0 (i.e., samples before aging), (b) 72, (c) 120, and (d) 600 h of aging. The molar ratios of AsO_4^{3-}/Fh were 0.004, 0.012, 0.02, and 0.1 for FhAS_a, FhAs_b, FhAs_c, and FhAs_d, respectively. These selected times provide the best visualization of Fh crystallization to Gt and Hm with time for the control Fh. After 600 h, the XRD patterns are very similar to those observed at 600 h. The same time points were selected for the rest of the sample series so that they could be directly compared with that observed for the control Fh.

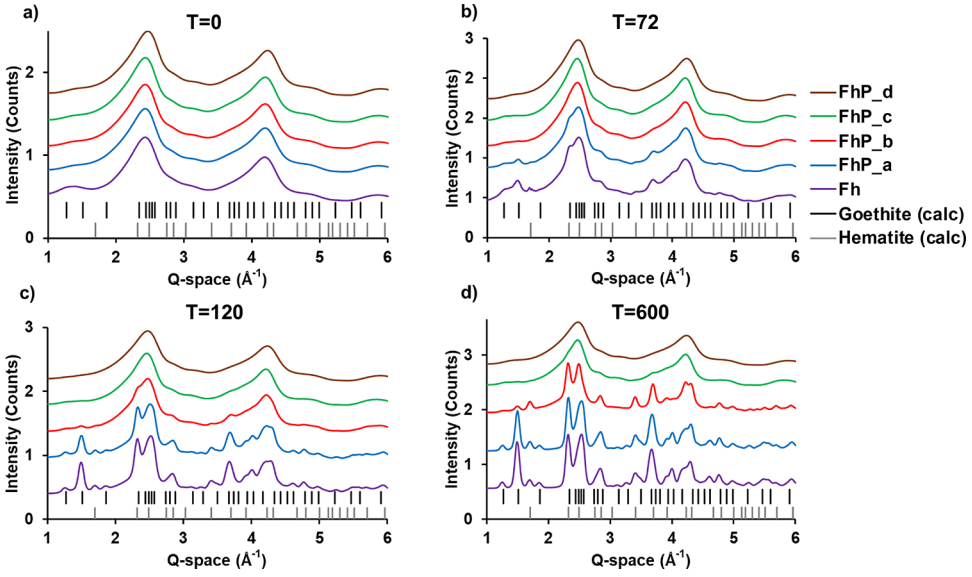

Figure 3. Synchrotron powder X-ray diffraction patterns for PO_4^{3-}-adsorbed samples at (a) 0 (i.e., fresh samples before aging), (b) 72, (c) 120, and (d) 600 h of aging. The molar ratios of/Fh were 0.004 for FhP_a, 0.012 for FhP_b, 0.02 for FhP_c, and 0.1 for FhP_d, respectively.

crystalline transformation products could be indexed to the known structures of Gt and/or Hm. The plot of measured intensity vs Q-space ($Q = \frac{4\pi\sin\theta}{\lambda}$; 2θ is the scattering angle and λ the incident wavelength) showed that this occurred with aging in all of the sample series, with the exception for FhAs_d and FhP_d (Figures 2 and 3). The changes in crystallinity were not identical for the different AsO_4^{3-}/Fh and PO_4^{3-}/Fh M ratios. For example, Gt and Hm formed more rapidly in control Fh and FhAs_a (0.004 M ratio) after 72 h, while crystallization was suppressed with increasing AsO_4^{3-} loading in FhAs_d (0.1 M ratio). A similar trend was observed in samples FhP_a and FhP_b with aging (Figure 3). Comparing the changes in the crystallinity of FhAs and FhP samples across different oxyanion surface loadings suggested that Fh transformation and crystallization were suppressed more in the presence of PO_4^{3-} compared with AsO_4^{3-}. This is evident by comparing samples FhAs_c (Figure 2) and FhP_c (Figure 3) at 600 h. The FhP_d sample (0.1 M ratio) did not show any crystallization similar to that observed for FhAa_d (Figures 2 and 3).

The fractions of the different phase(s) present were quantified by using LCF of the real-space PDFs. The PDF profiles and LCF fit for selected samples are shown in Figures S1−S3. Figure 4 shows the results of LCF analysis for different sample series. The transformation of Fh decreased in the presence of AsO_4^{3-} such that the Fh abundance at t = 1200 h varied from 12.2 ± 0.41% for control Fh to 98.2 ± 0.04% for FhAs_d (Table 1). Goethite formation was inhibited in the presence of AsO_4^{3-} and decreased from 64.5 ± 0.33% for the control Fh to 9.4 ± 0.30 for FhAs_c in the t = 1200 h. Goethite was not formed in the FhAs_d sample with the highest AsO_4^{3-}/Fh loading (0.1 M ratio). For the FhAs sample, the abundance of Hm increased from 23.3 ± 0.11% for

https://doi.org/10.1021/acsearthspacechem.3c00232
ACS Earth Space Chem. XXXX, XXX, XXX−XXX

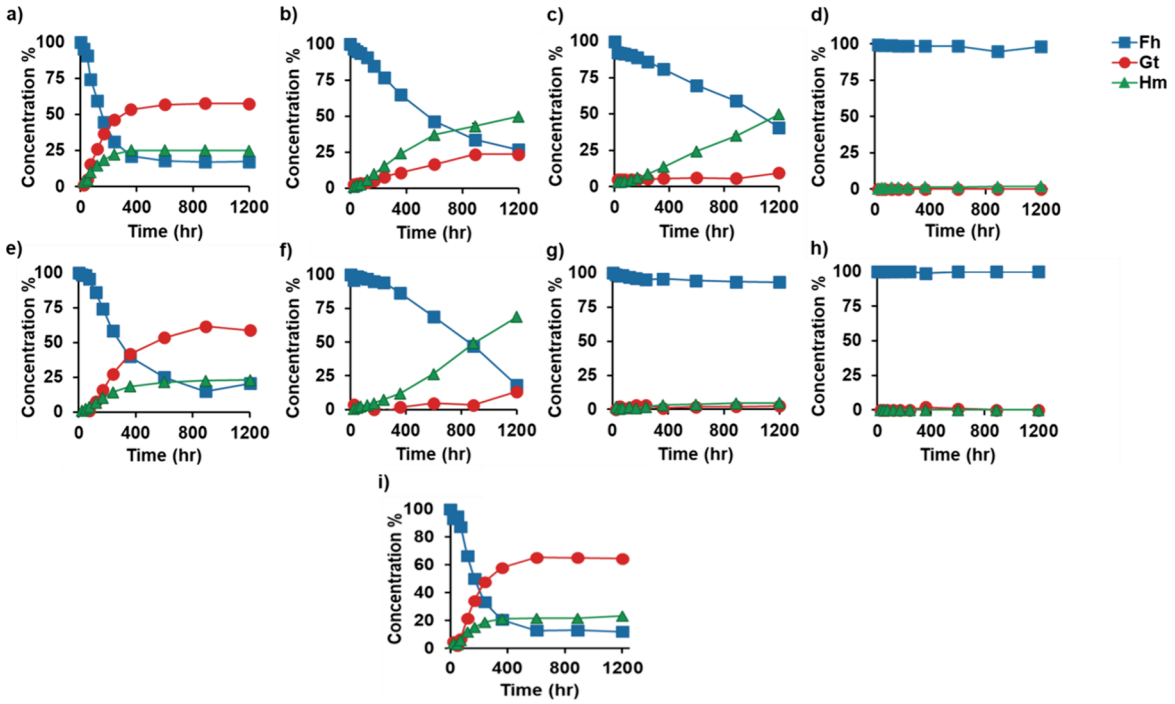

Figure 4. Quantified fraction of Fh, Gt, and Hm with time for (a) FhAs_a, (b) FhAs_b, (c) FhAs_c, (d) FhAs_d, (e) FhP_a, (f) FhP_b, (g) FhP_c, (h) FhP_d, and (i) control Fh. Error bars representing the standard error are smaller than the symbols (n = 3). The AsO_4^{3-} and PO_4^{3-}/Fh molar ratios were 0.004 for FhAS_a and FhP_a, 0.012 for FhAs_b and FhP_b, 0.02 for FhAs_c and FhP_c, and 0.1 for FhAs_d and FhP_d, respectively.

Table 1. Fraction of Transformation Products in the t = 1200 h

Sample	Fh %	Gt %	Hm %	Hm/Gt + Hm
control Fh	12.2 (0.41)[a]	64.5 (0.33)	23.3 (0.11)	0.27 (0.07)
FhAs_a	17.4 (0.12)	57.6 (0.06)	25.0 (0.14)	0.30 (0.07)
FhAs_b	26.7 (0.37)	23.5 (0.27)	49.8 (0.09)	0.68 (0.04)
FhAs_c	40.8 (0.65)	9.4 (0.30)	49.8 (0.36)	0.84 (0.09)
FhAs_d	98.2 (0.04)	0.00	1.8 (0.04)	1.00 (0.14)
FhP_a	20.5 (1.27)	58.7 (0.89)	23.0 (0.38)	0.28 (0.13)
FhP_b	18.0 (0.70)	13.4 (0.18)	68.8 (0.56)	0.84 (0.09)
FhP_c	93.4 (0.42)	2.5 (0.03)	4.7 (0.04)	0.65 (0.09)
FhP_d	100	0.00	0.00	–[b]

[a]Numbers in parentheses correspond to the standard error (n = 3). [b]No significant transformation detected.

control Fh to 49.8 ± 0.36% for FhAs_c at t = 1200 h. The abundance of Hm was 1.8 ± 0.04% for FhAs_d (Table 1). The $\frac{Hm}{Hm + Gt}$ ratio increased by increasing the AsO_4^{3-} surface loading, ranging from 0.27 ± 0.07 for control Fh to 0.84 ± 0.09 for FhAs_c. Although the $\frac{Hm}{Hm + Gt}$ ratio for FhAs_d was 1.00 ± 0.14, this value could be misleading because the only product of transformation was 1.84 ± 0.04% Hm. This suggests that the sample would need to be aged longer in order to have more Fh transformation and a more accurate $\frac{Hm}{Hm + Gt}$ ratio (Table 1).

Phosphate surface loading also had a significant impact on Fh transformation behavior. The Fh fractions in t = 1200 h ranged from 12.2 ± 0.41 for control Fh to 93.4 ± 0.42% for FhP_c. The Gt fraction decreased from 64.5 ± 0.33% for control Fh to 13.4 ± 0.18% for FhP_b, whereas the Hm fraction increased from 23.3 ± 0.11% for control Fh to 68.8 ± 0.56% for FhP_b. The Gt (2.51 ± 0.03%) and Hm (4.70 ± 0.04%) fractions were very low in the FhP_c sample, suggesting that a longer aging time was required for this sample to transform completely. The samples with the highest PO_4^{3-} loadings (FhP_d) did not show any transformation with aging.

The $\frac{Hm}{Hm + Gt}$ ratio increased with increasing the PO_4^{3-} surface loading in the samples that showed at least 10% Fh transformation. This ratio increased linearly from 0.27 ± 0.07 for control Fh to 0.84 ± 0.09 for FhP_b (Table 1). The impact of oxyanion surface loading on the $\frac{Hm}{Hm + Gt}$ ratio was more significant in the presence of PO_4^{3-} than AsO_4^{3-}. For example, for the 0.02 AsO_4^{3-}/ Fh M ratio (FhAs_c sample), the $\frac{Hm}{Hm + Gt}$ value was 0.84 (0.09), while the same value was achieved in the presence of a significantly lower PO_4^{3-}/ Fh M ratio (0.012; FhP_b) (Table 1).

Rate of Transformation. The transformation of Fh to Gt and Hm follows a pseudo-first-order kinetic reaction described in Namayandeh et al.[71] The rate law derivation is provided in Text S3. The following reaction was used to determine the rate of the Fh transformation.

$$\ln[Fh]_t = \ln[Fh]_0 - (k_{Gt} + k_{Ht})t \quad (1)$$

where $[Fh]_t$ and $[Fh]_0$ are the concentration of Fh at time t and 0, respectively, k_{Gt} and k_{Hm} are the rate constant of Gt and Hm formation, and t is time. The plot of ln $[Fh]t$ vs time gives a straight line with a slope of $-(k_{Gt} + k_{Hm})$ (Figure 5). The slope of the lines decreased from 3.76×10^{-3} ± 1.1 for control Fh to 4.91×10^{-4} ± 1.0×10^{-5} for FhAs_c and 7.30×10^{-5} ± 5.4×10^{-6} for FhP_c (Figure 5).

Reaction 2 was written based on the formation of Gt

https://doi.org/10.1021/acsearthspacechem.3c00232
ACS Earth Space Chem. XXXX, XXX, XXX−XXX

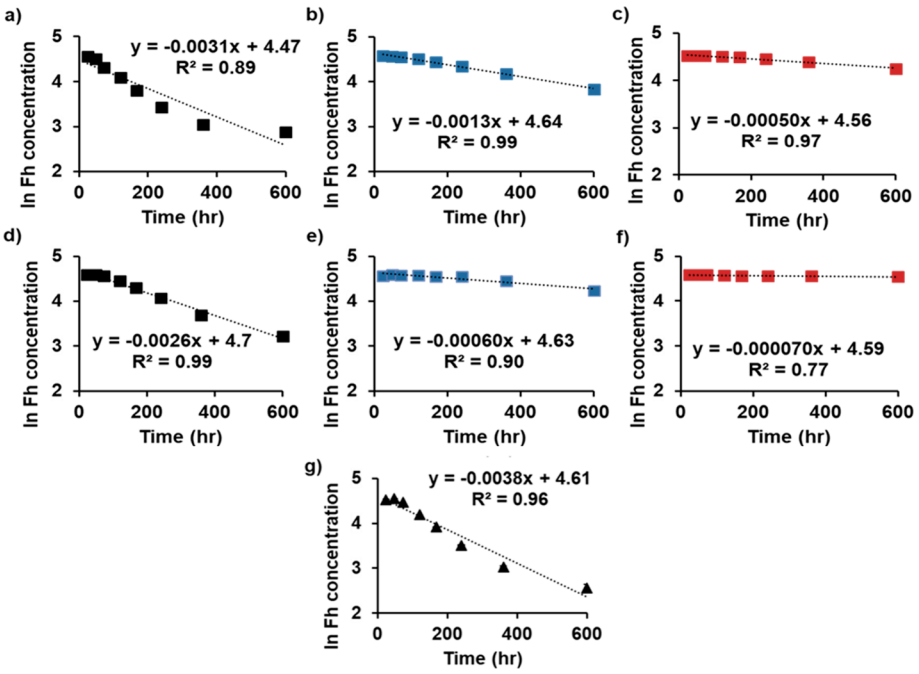

Figure 5. Ln *F*h concentration vs time for (a) FhAs_a, (b) FhAs_b, (c) FhAs_c, (d) FhP_a, (e) FhP_b, (f) FhP_c, and (g) control Fh. The slope of the line equals $-(k_{Gt} + K_{Hm})$, where $k_{Gt} + K_{Hm}$ is the rate constant of Gt and Hm formation, respectively.

Table 2. Pseudo-First-Order Kinetic Parameters for Fh Transformation

sample	$Gt_{600\ h}$ [a] (%)	$Hm_{600\ h}$ (%)	slope $-(k_{Gt} + k_{Hm})$	k_{Gt}/k_{Hm}	k_{Gt} (h^{-1})	k_{Hm} (h^{-1})
control Fh	65.3 (0.01)[b]	21.6 (0.07)	3.76 (1.1×10^{-4})	3.02 (1.6×10^{-2})	2.83×10^{-3} (1.1×10^{-4})	9.35×10^{-4} (2.7×10^{-5})
FhAs_a	57.6 (0.06)	25.0 (0.1)	3.14×10^{-3} (1.5×10^{-4})	2.26 (5.1×10^{-3})	2.18×10^{-3} (1.6×10^{-4})	9.62×10^{-4} (4.7×10^{-5})
FhAs_b	23.5 (0.3)	49.8 (0.1)	1.30×10^{-3} (1.6×10^{-5})	0.441 (4.4×10^{-3})	3.98×10^{-3} (2.1×10^{-5})	9.01×10^{-4} (1.4×10^{-5})
FhAs_c	9.4 (0.3)	49.8 (0.3)	4.91×10^{-4} (1.0×10^{-5})	0.251 (4.7×10^{-3})	9.87×10^{-5} (1.6×10^{-5})	3.93×10^{-4} (1.1×10^{-5})
FhP_a	58.7 (0.9)	23.0 (0.4)	2.60×10^{-3} (3.7×10^{-5})	2.48 (9.2×10^{-2})	1.82×10^{-3} (4.8×10^{-5})	7.31×10^{-4} (2.9×10^{-5})
FhP_b	13.4 (0.2)	68.8 (0.6)	5.90×10^{-4} (2.7×10^{-5})	0.173 (2.1×10^{-3})	8.65×10^{-5} (3.6×10^{-5})	5.00×10^{-4} (2.4×10^{-5})
FhP_c	2.5 (0.4)	4.7 (0.04)	7.30×10^{-5} (5.4×10^{-6})	0.537 (9.6×10^{-3})	2.55×10^{-5} (6.6×10^{-6})	4.75×10^{-5} (3.6×10^{-6})

[a]It is the time needed for the transformation of control Fh to reach completion. [b]Numbers in parentheses represent the standard error (n = 3).

$$\frac{d[Gt]}{dt} = k_{Gt}[Fh]_t[H^+] \quad (2)$$

In this work, H^+ concentration was buffered; thus, it can be canceled out. Also, we can write the rate law for Hm formation as

$$\frac{d[Hm]}{dt} = k_{Hm}[Fh]_t \quad (3)$$

We take the ratio of these two reactions

$$\frac{\frac{d[Gt]}{dt}}{\frac{d[Hm]}{dt}} = \frac{k_{Gt}[Fh]}{k_{Hm}[Fh]} \quad (4)$$

The integration of this ratio provides the relationship for calculating the rate constant of Gt and Hm formation

$$\frac{K_{Gt}}{K_{Ht}} = \frac{[Gt_{600\ h}]}{[Hm_{600\ h}]} \quad (5)$$

where $Gt_{600\ h}$ and $Hm_{600\ h}$ are the Gt and Hm concentrations at t = 600 h, respectively. The $t_{600\ h}$ is the time needed for the control Fh to transform completely. Using the slope of the line $\{-(k_{Gt} + k_{Hm})\}$ from eqs 1 and 5, the Gt and Hm rate constants can be calculated (Table 2). The high R^2 of the graph of Ln Fh concentration vs time, even in the presence of oxyanion, for the transformed samples proposed that the primary rate-limiting step is the concentration of Fh (Figure 5). This suggests that this model can be used for complex systems, such as soils that contain impurities. Figure 6 shows

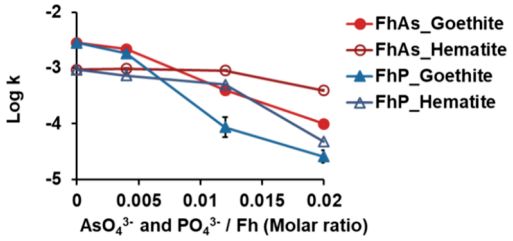

Figure 6. Variation on the log of Hm and Gt rate constants with AsO_4^{3-} and PO_4^{3-} surface loading.

the plot of log k_{Gt} and k_{Hm} vs AsO_4^{3-} and PO_4^{3-}/Fh M ratio. The rate constants of both Gt and Hm formation decreased with increasing AsO_4^{3-} and PO_4^{3-} surface loading. The rate constant of Gt formation was higher than that of Hm for control Fh, FhAs_a, and FhP_a samples but it decreased below the rate of Hm formation for FhAs_b, FhAs_c, FhP_b, and FhP_c. Although both FhAs and FhP samples showed the

https://doi.org/10.1021/acsearthspacechem.3c00232
ACS Earth Space Chem. XXXX, XXX, XXX−XXX

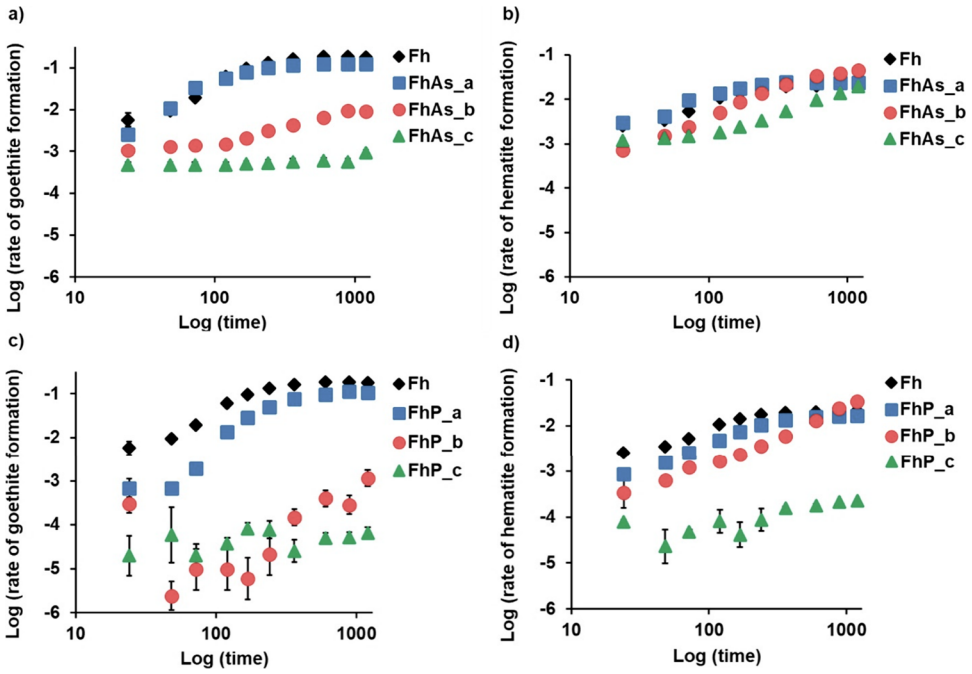

Figure 7. Rates of Gt and Hm formation across different surface loadings. The error bars represent the standard error (n = 3). Error bars for some samples are smaller than the symbol and are not seen. The rate of Gt and Hm formation was plotted logarithmically to show the differences in the early stage of transformation.

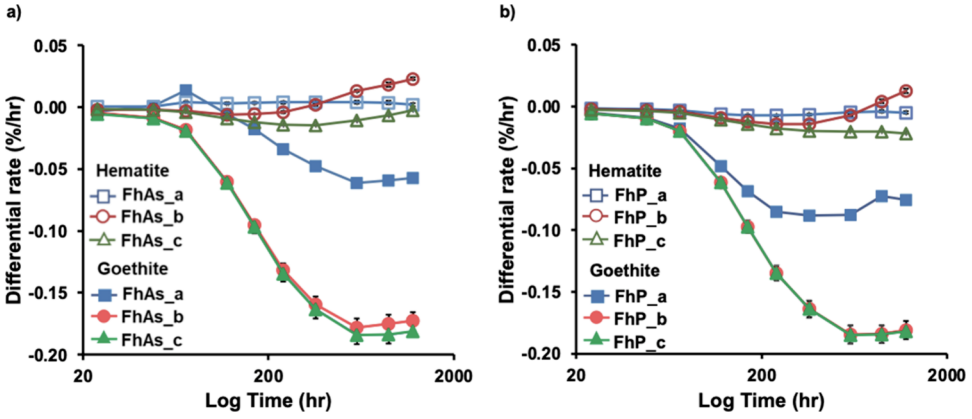

Figure 8. Differential rate of Hm and Gt formation calculated by subtracting the rate of the Fh control for a) AsO_4^{3-} and b) PO_4^{3-} adsorbed samples. Positive and negative values show rates faster or slower than the control rate. Zero values equal the rate of control Fh. "Differential rate" was called "corrected rate" in Namayandeh et al.[71]

same trend, the rate constants for the FhP samples were significantly lower than those of the FhAs samples (Figure 6).

The obtained rate constant values were used in the following equations to calculate the rates of Gt and Hm formation

$$\frac{d[Gt]}{dt} = k_{Gt}[Fh]_t \quad (6)$$

$$\frac{d[Hm]}{dt} = k_{Hm}[Fh]_t \quad (7)$$

The log−log plots of Gt and Hm formation rate versus time showed that increasing the oxyanion surface loading inhibits the formation of Gt and Hm (Figure 7). The FhAs_a sample with the lowest AsO_4^{3-} loading (AsO_4^{3-}/ Fh M ratio = 0.004) showed almost the same Gt and Hm formation rate as the control Fh. The rate of Gt formation decreased significantly with increased AsO_4^{3-} surface loading as shown by FhAs_b (0.012 AsO_4^{3-}/ Fh M ratio) and FhAs_c (0.02 AsO_4^{3-}/ Fh M ratio) samples. As stated, the rate of Hm formation was delayed initially with increased AsO_4^{3-} surface loading; however, unlike Gt formation, it progressively increased with time to that of control Fh by the end of the experiment (Figure 7). Although the rate model revealed a similar pattern of Gt formation for FhP samples, the impact of PO_4^{3-} on the Fh transformation was greater than that of AsO_4^{3-} (Figure 4). At the early stage of transformation, the rate of Gt formation for the FhP_a sample was repressed, but it reached that of control Fh at the late stage of transformation. The rate of Gt formation was suppressed for FhP_b (PO_4^{3-}/Fh= 0.02) and FhP_c (PO_4^{3-}/Fh= 0.1). Although the rate of Hm formation was slow at the early stage of the experiment for FhP_a and FhP_b, it increased steadily with aging, until it eventually reached that of control Fh. The rate of Hm formation was largely suppressed in FhP_c samples and was approximately constant with aging.

https://doi.org/10.1021/acsearthspacechem.3c00232
ACS Earth Space Chem. XXXX, XXX, XXX−XXX

The rate of Gt and Hm formation for control Fh was subtracted from that of adsorbed samples to compare the impact of oxyanion surface loading on the rate of Gt and Hm formation. As shown in Figure 8, AsO_4^{3-} and PO_4^{3-} adsorption decreased the rate of Gt formation in all of the samples and had the greatest impact on the samples with the highest surface loading (0.0012 and 0.02 molar ratio). The impact of AsO_4^{3-} and PO_4^{3-} adsorption on the rate of Hm formation was almost negligible for FhAs_a and FhP_a (~0.004 molar ratio). For both FhAs_b and FhP_b, the rate of Hm formation initially decreased with aging, but it increased beyond that of the control, starting after ~200 h. Likewise, for FhAs_c with the highest surface loading (0.02 molar ratio), the rate of Hm formation decreased in the early stage of transformation and progressively increased to that of control Fh. However, the resulting product never became positive. The differential rate shows that the rate of Hm formation decreased for the FhP_c sample, but unlike FhAs_c, it never increased to that of the Fh control by the end of aging. The differential rate of Hm and Gt formation suggests that PO_4^{3-} has a stronger impact on the rate of Fh transformation compared to AsO_4^{3-}.

Pathways of Fh Transformation. Two major pathways have been suggested for the transformation of Fh to Gt and Hm.[27,72] In the first pathway, metastable Fh particles undergo dissolution and recrystallize as transformation products.[28,82] In the other pathway, Fh particles can aggregate through oriented attachment (OA) and form the products.[28,72,83−86] The presence of AsO_4^{3-} and PO_4^{3-} on the Fh surface increased the level of formation of Hm over Gt. Surface complexation modeling showed that AsO_4^{3-} and PO_4^{3-} directly bond on Fh through inner-sphere complexes that involve displacing water from the Fh surface. Decreasing the degree of surface hydration reduces Fh dissolution and, therefore, the subsequent formation of products through dissolution/recrystallization. The fraction of Gt decreased with increasing AsO_4^{3-} and PO_4^{3-} surface loading (Figure 4), which suggests that Gt formation is mainly through dissolution/recrystallization. This is consistent with previous studies that reported this pathway as the primary mechanism for the formation of Gt during the transformation of 2-line Fh in different chemical conditions.[27,28,82,87,88]

Arsenate and PO_4^{3-} adsorption on Fh through inner-sphere complexes promoted Hm formation during Fh transformation. The hydration sphere of oxyanion is removed during their inner-sphere complexation on the Fh surface.[1,68−70] This removes water from the interfaces and facilitates the aggregation of particles by OA as suggested by Yuwono et al.[89] In addition, removing the hydration sphere is followed by the inner-sphere adsorption of oxyanion that consumes positive charges on the Fh surface, which, in turn, decreases the electrostatic repulsion on the surface and induces aggregation by OA.[90] This is consistent with the Derjaguin, Landau, Verwey, and Overbeek (DLVO) theory showing faster particle aggregation with decreasing surface protonation.[90−93]

High surface loadings of AsO_4^{3-} and PO_4^{3-} (0.1 M ratio) stabilized Fh and inhibited transformation (Figure 4). The nucleation of Gt and Hm requires at least a degree of hydration within the aggregates.[72] The extreme dehydration of the Fh surface in the presence of high AsO_4^{3-} and PO_4^{3-} surface loading inhibits the nucleation of new phases during Fh transformation. In addition, strongly adsorbed AsO_4^{3-} and PO_4^{3-} inhibit aggregation by OA by populating the interfaces between adjoining Fh particles.[89]

Although the mechanism of AsO_4^{3-} and PO_4^{3-} adsorption on Fh has been reported to be similar,[12,53,54,56,57,59] PO_4^{3-} showed stronger effects in decreasing the rate and inducing Hm formation. This agrees with the results reported by Bolanz et al.,[24] who showed that at pH 4 and 7, the induction time was longer, and more Hm was formed in the presence of adsorbed PO_4^{3-}, compared to AsO_4^{3-}. There is a tension in the literature about the affinity of AsO_4^{3-} and PO_4^{3-} for adsorption on iron oxyhydroxides (e.g., Gt). While some studies reported higher adsorption of AsO_4,[3−56,94] some other studies showed that PO_4[3−55,59,95,96] is more strongly adsorbed on iron oxyhydroxides. Antelo et al.[53] reported that PO_4^{3-} is more sensitive to changes in pH and ionic strength. They showed that PO_4^{3-} adsorption increases in acidic pH at different ionic strengths and decreases at basic pH and low ionic strengths, compared to AsO_4.[3−53] Therefore, the AsO_4^{3-} and PO_4^{3-} adsorption on iron oxy-hydroxides depends on the system chemistry and may not be identical under different chemical conditions.[58] In addition, Langmuir[97] proposed that smaller ions with higher charges, that is, with a higher ionic potential (IP = Z/r), show a higher affinity for forming a strong covalent bond on the surface of solids. The IP of the PO_4^{3-} ion (1.26) is slightly higher than that of AsO_4^{3-} (1.21), leading to a higher adsorption capacity for PO_4^{3-} (5.03 μmol/m^2) than AsO_4^{3-} (4.18 μmol/m^2) reported by Bolanz et al.[24]

Using DFT calculations, we showed that the Fh surface is dehydrated through AsO_4^{3-} and PO_4^{3-} inner-sphere complexes. Surface dehydration impacts the rate and pathway of Fh transformation, in part, by suppressing the dissolution/precipitation pathway through which the metastable Fh particles dissolve and precipitate as products. This was evidenced by the significant decrease in the Gt formation with increased surface loading. Additionally, oxyanions remove the hydration sphere between them and the surface, share electrons with Fe^{3+}, and balance the positive charge on the surface, which promotes particle aggregation through OA. Note that different oxyanions do not have the same strength to remove the hydration sphere, which controls their potential for balancing the positive charges on the surface and, thus, the aggregation of particles. For example, unlike AsO_4^{3-} and PO_4^{3-}, NO_3^- predominantly forms weak outer-sphere complexes on Fh[9,47,98] where the hydration sphere can not be removed during adsorption, resulting in less charge consumption on the surface. Decreasing the degree of hydration and positive charges on the Fh surface showed a positive correlation with the formation of Hm, suggesting that Hm is primarily formed through dehydration/aggregation, which is consistent with a previous study.[22]

In summary, we showed the impact of oxyanion surface loading on the rate and pathway of Fh transformation. AsO_4^{3-} and PO_4^{3-} adsorption showed similar effects, although PO_4^{3-} had a stronger influence on the transformation process. Both oxyanions decreased the rate of transformation and promoted the formation of Hm, which positively correlated with increased surface loading. Although our data suggested that Gt and Hm are formed through dissolution/recrystallization and dehydration/aggregation, respectively, this work cannot directly show the mechanism of Fh transformation. Further studies using cryogenic transmission electron microscopy are needed to elucidate the impact of different oxyanion surface complexes and loading on the mechanism of Fh transformation.

https://doi.org/10.1021/acsearthspacechem.3c00232
ACS Earth Space Chem. XXXX, XXX, XXX−XXX

CONCLUSIONS

This work shows the impact of oxyanion surface loading on the rate and pathway of Fh transformation. We showed that increasing AsO_4^{3-} and PO_4^{3-} adsorption on Fh inhibited Gt formation and induced Hm formation. We suggested that these oxyanions dehydrate the Fh surface through inner-sphere complexes, which delays the dissolution/recrystallization pathway and promotes aggregation, resulting in increased Hm formation. oxyanion adsorption also decreases the positive charges on the Fh surface, which in turn decreases the repulsion between particles and promotes the aggregation pathway of transformation. The kinetic model showed that the rate of Fh transformation drastically decreased with oxyanion surface loading such that the Fh transformation was completely inhibited at the highest surface loading (0.1 M ratio). Phosphate adsorption had a stronger effect on Fh transformation compared to AsO_4^{3-}, which may be attributed to its higher IP and adsorption capacity on Fh. Also, our results showed that AsO_4^{3-} and PO_4^{3-} remained on the Fh surface during transformation, which we attribute to their strong affinity for the Fh surfaces as well as those of the transformation products. The results of this work have implications for understanding the formation of natural nanoparticles, their reactivity toward contaminants and nutrients, and the impacts of these species on nanoparticle transformations under Earth-surface environmental conditions.

ASSOCIATED CONTENT

Supporting Information

The Supporting Information is available free of charge at https://pubs.acs.org/doi/10.1021/acsearthspacechem.3c00232.

Experimental conditions and oxyanion species for each corresponding experiment; surface complexation model; Surface complexation reactions, equilibrium constants, and plane charge distribution; density function theory calculation; lists of bonds and H-bonds for $HAsO_4^{2-}$ aqueous Fh and AsO_4^{3-} inner-sphere complexation on Fh; lists of bonds and H-bonds for HPO_4^{2-} aqueous Fh and PO_4^{3-} inner-sphere complexation on Fh; AsO_4^{3-}-adsorbed samples at various times of aging; and PO_4^{3-}-adsorbed samples at various times of aging; LCF fit for Fh control samples at various times of aging (PDF)

AUTHOR INFORMATION

Corresponding Author

Alireza Namayandeh − *Department of Geosciences, Virginia Tech, Blacksburg, Virginia 24061, United States; Department of Earth System Science, Stanford University, Stanford, California 94305, United States;* orcid.org/0000-0003-2942-3245; Email: arnama@stanford.edu

Authors

Olaf J. Borkiewicz − *Advanced Photon Source, Argonne National Laboratory, Lemont, Illinois 60439, United States*

Nefeli M. Bompoti − *Department of Civil and Environmental Engineering, University of Connecticut, Storrs, Connecticut 06269, United States;* orcid.org/0000-0003-2799-188X

Steven K. Watson − *Department of Geosciences, Virginia Tech, Blacksburg, Virginia 24061, United States*

James D. Kubicki − *Department of Earth, Environmental & Resource Sciences, The University of Texas at El Paso, El Paso, Texas 79968, United States;* orcid.org/0000-0002-9277-9044

Maria Chrysochoou − *Department of Civil and Environmental Engineering, University of Connecticut, Storrs, Connecticut 06269, United States*

F. Marc Michel − *Department of Geosciences and Division of Nanoscience, Academy of Integrated Science, Virginia Tech, Blacksburg, Virginia 24061, United States*

Complete contact information is available at: https://pubs.acs.org/10.1021/acsearthspacechem.3c00232

Notes

The authors declare no competing financial interest.

ACKNOWLEDGMENTS

F.M.M. gratefully acknowledges financial support provided by the National Science Foundation through CAREER-1652237. This work used shared facilities at the Nanoscale Characterization and Fabrication Laboratory, which is funded and managed by Virginia Tech's Institute for Critical Technology and Applied Science. Additional support is provided by the Virginia Tech National Center for Earth and Environmental Nanotechnology Infrastructure (NanoEarth), a member of the National Nanotechnology Coordinated Infrastructure (NNCI), supported by NSF (ECCS 1542100 and ECCS 2025151). This research used resources from the Advanced Photon Source, a U.S. Department of Energy (DOE) Office of Science User Facility operated for the DOE Office of Science by the Argonne National Laboratory under Contract No. DE-AC02-06CH11357.

REFERENCES

(1) Gu, C.; Wang, Z.; Kubicki, J. D.; Wang, X.; Zhu, M. X-ray Absorption Spectroscopic Quantification and Speciation Modeling of Sulfate Adsorption on Ferrihydrite Surfaces. *Environ. Sci. Technol.* **2016**, *50* (15), 8067−8076.

(2) Adra, A.; Morin, G.; Ona-Nguema, G.; Brest, J. arsenate and arsenite adsorption onto Al-containing ferrihydrites. Implications for arsenic immobilization after neutralization of acid mine drainage. *Appl. Geochem.* **2016**, *64*, 2.

(3) Antelo, J.; Arce, F.; Fiol, S. arsenate and phosphate adsorption on ferrihydrite nanoparticles. Synergetic interaction with calcium ions. *Chem. Geol.* **2015**, *410*, 53−62.

(4) Zhu, M.; Northrup, P.; Shi, C.; Billinge, S. J.; Sparks, D. L.; Waychunas, G. A. Structure of sulfate adsorption complexes on ferrihydrite. *Environ. Sci. Technol. Lett.* **2014**, *1* (1), 97.

(5) Johnston, C. P.; Chrysochoou, M. Investigation of chromate coordination on ferrihydrite by in situ ATR-FTIR spectroscopy and theoretical frequency calculations. *Environ. Sci. Technol.* **2012**, *46* (11), 5851.

(6) Antelo, J.; Fiol, S.; Pérez, C.; Mariño, S.; Arce, F.; Gondar, D.; López, R. Analysis of phosphate adsorption onto ferrihydrite using the CD-MUSIC model. *J. Colloid Interface Sci.* **2010**, *347* (1), 112−119.

(7) Carabante, I.; Grahn, M.; Holmgren, A.; Kumpiene, J.; Hedlund, J. Adsorption of As (V) on iron oxide nanoparticle films studied by in situ ATR-FTIR spectroscopy. *Colloids Surf., A* **2009**, *346* (1), 106−113.

(8) Arai, Y.; Sparks, D. L. ATR−FTIR Spectroscopic Investigation on Phosphate Adsorption Mechanisms at the Ferrihydrite−Water Interface. *J. Colloid Interface Sci.* **2001**, *241* (2), 317−326.

(9) Sparks, D. L., Fundamentals of Soil Chemistry. In *Encyclopedia of Water: Science, Technology, and Society*; 2019; pp 1−11.

(10) Sparks, D. L. *Environmental soil chemistry*, 2nd ed.; Academic: San Diego, Calif., London, 2003.

(11) Tian, L.; Shi, Z.; Lu, Y.; Dohnalkova, A. C.; Lin, Z.; Dang, Z. Kinetics of Cation and oxyanion Adsorption and Desorption on Ferrihydrite: Roles of Ferrihydrite Binding Sites and a Unified Model. *Environ. Sci. Technol.* **2017**, *51* (18), 10605−10614.
(12) Hiemstra, T.; Zhao, W. Reactivity of ferrihydrite and ferritin in relation to surface structure, size, and nanoparticle formation studied for phosphate and arsenate. *Environ. Sci.: Nano* **2016**, *3* (6), 1265−1279.
(13) Sposito, G. *The Chemistry of Soils*; Oxford University Press: New York, 1987.
(14) Namayandeh, A.; Kabengi, N. Calorimetric study of the influence of aluminum substitution in ferrihydrite on sulfate adsorption and reversibility. *J. Colloid Interface Sci.* **2019**, *540*, 20−29.
(15) Michel, F. M.; Barrón, V.; Torrent, J.; Morales, M. P.; Serna, C. J.; Boily, J. F.; Liu, Q.; Ambrosini, A.; Cismasu, A. C.; Brown, G. E. Ordered ferrimagnetic form of ferrihydrite reveals links among structure, composition, and magnetism. *Proc. Natl. Acad. Sci. U. S. A.* **2010**, *107* (7), 2787.
(16) Sheng, A.; Liu, J.; Li, X.; Qafoku, O.; Collins, R. N.; Jones, A. M.; Pearce, C. I.; Wang, C.; Ni, J.; Lu, A.; Rosso, K. M. Labile Fe(III) from sorbed Fe(II) oxidation is the key intermediate in Fe(II)-catalyzed ferrihydrite transformation. *Geochim. Cosmochim. Acta* **2020**, *272*, 105−120.
(17) Ye, C.; Ariya, P. A.; Fu, F.; Yu, G.; Tang, B. Influence of Al(III) and Sb(V) on the transformation of ferrihydrite nanoparticles: Interaction among ferrihydrite, coprecipitated Al(III) and Sb(V). *J. Hazard. Mater.* **2021**, *408*, No. 124423.
(18) ThomasArrigo, L. K.; Kaegi, R.; Kretzschmar, R. Ferrihydrite Growth and Transformation in the Presence of Ferrous Iron and Model Organic Ligands. *Environ. Sci. Technol.* **2019**, *53* (23), 13636−13647.
(19) Lu, Y.; Hu, S.; Wang, Z.; Ding, Y.; Lu, G.; Lin, Z.; Dang, Z.; Shi, Z. Ferrihydrite transformation under the impact of humic acid and Pb: kinetics, nanoscale mechanisms, and implications for C and Pb dynamics. *Environ. Sci.: Nano* **2019**, *6* (3), 747−762.
(20) Hu, S.; Lu, Y.; Peng, L.; Wang, P.; Zhu, M.; Dohnalkova, A. C.; Chen, H.; Lin, Z.; Dang, Z.; Shi, Z. Coupled kinetics of ferrihydrite transformation and As (V) sequestration under the effect of humic acids: a mechanistic and quantitative study. *Environ. Sci. Technol.* **2018**, *52* (20), 11632−11641, DOI: 10.1021/acs.est.8b03492.
(21) Zhang, D.; Wang, S.; Wang, Y.; Gomez, M. A.; Duan, Y.; Jia, Y. The transformation of two-line ferrihydrite into crystalline products: effect of pH and media (sulfate versus nitrate). *ACS Earth Space Chem.* **2018**, *2* (6), 577−587.
(22) Soltis, J. A.; Feinberg, J. M.; Gilbert, B.; Penn, R. L. Phase Transformation and Particle-Mediated Growth in the Formation of Hematite from 2-Line Ferrihydrite. *Cryst. Growth Des.* **2016**, *16* (2), 922−932.
(23) Shimizu, M.; Zhou, J.; Schröder, C.; Obst, M.; Kappler, A.; Borch, T. Dissimilatory reduction and transformation of ferrihydrite-humic acid coprecipitates. *Environ. Sci. Technol.* **2013**, *47* (23), 13375−13384.
(24) Michael Bolanz, R.; Bläss, U.; Ackermann, S.; Ciobotă, V.; Rösch, P.; Tarcea, N.; Popp, J.; Majzlan, J. J. C.; Minerals, C. The effect of antimonate, arsenate, and phosphate on the transformation of ferrihydrite to goethite, hematite, feroxyhyte, and tripuhyite. *Clays Clay Miner* **2013**, *61* (1), 11−25.
(25) Das, S.; Hendry, M. J.; Essilfie-Dughan, J. Transformation of two-line ferrihydrite to goethite and hematite as a function of pH and temperature. *Environ. Sci. Technol.* **2011**, *45* (1), 268−275.
(26) Das, S.; Hendry, M. J.; Essilfie-Dughan, J. Effects of adsorbed arsenate on the rate of transformation of 2-line ferrihydrite at pH 10. *Environ. Sci. Technol.* **2011**, *45* (13), 5557−5563.
(27) Cudennec, Y.; Lecerf, A. The transformation of ferrihydrite into goethite or hematite, revisited. *J. Solid State Chem.* **2006**, *179* (3), 716−722.
(28) Schwertmann, U.; Stanjek, H.; Becher, H. H. Long-term in vitro transformation of 2-line ferrihydrite to goethite/hematite at 4, 10, 15 and 25°C. *Clay Miner.* **2004**, *39* (4), 433−438.
(29) Johnston, J. H.; Lewis, D. G. A detailed study of the transformation of ferrihydrite to hematite in an aqueous medium at 92°C. *Geochim. Cosmochim. Acta* **1983**, *47* (11), 1823−1831.
(30) Chen, S. A.; Heaney, P. J.; Post, J. E.; Eng, P. J.; Stubbs, J. E. Hematite-goethite ratios at pH 2−13 and 25−170 °C: A time-resolved synchrotron X-ray diffraction study. *Chem. Geol.* **2022**, *606*, No. 120995.
(31) Chen, S. A.; Heaney, P. J.; Post, J. E.; Fischer, T. B.; Eng, P. J.; Stubbs, J. E. Superhydrous hematite and goethite: A potential water reservoir in the red dust of Mars? *Geology* **2021**, *49*, 1343.
(32) Das, S.; Essilfie-Dughan, J.; Hendry, M. J. J. C. G., Fate of adsorbed arsenate during phase transformation of ferrihydrite in the presence of gypsum and alkaline conditions. *Chem. Geol.* 2015, *411*, 69−80 DOI: 10.1016/j.chemgeo.2015.06.031.
(33) Han, J.; Kim, M.; Ro, H.-M. J. E. C. L. Factors modifying the structural configuration of oxyanions and organic acids adsorbed on iron (hydr) oxides in soils. A review. *Environ. Chem. Lett.* **2020**, *18* (3), 631−662.
(34) Han, J.; Kim, M.; Ro, H.-M. Factors modifying the structural configuration of oxyanions and organic acids adsorbed on iron (hydr) oxides in soils. A review. *Environ. Chem. Lett.* **2020**, 18−631, DOI: 10.1007/s10311-020-00964-4.
(35) Schaefer, M. V.; Ying, S. C.; Benner, S. G.; Duan, Y.; Wang, Y.; Fendorf, S. J. E. S. Aquifer arsenic cycling induced by seasonal hydrologic changes within the Yangtze River Basin. *Environ. Sci. Technol.* **2016**, *50* (7), 3521−3529.
(36) Stuckey, J. W.; Schaefer, M. V.; Benner, S. G.; Fendorf, S. J. G. E. C. A. Reactivity and speciation of mineral-associated arsenic in seasonal and permanent wetlands of the Mekong Delta. *Geochim. Cosmochim. Acta* **2015**, *171*, 143−155.
(37) Wang, H.; Göttlicher, J.; Byrne, J.; Guo, H.; Benning, L. G.; Norra, S. J. J.; O, H. M., Vertical redox zones of Fe−S−As coupled mineralogy in the sediments of Hetao Basin−Constraints for groundwater As contamination. *J. Hazard. Mater.* 2021, *408*, 124924, DOI: 10.1016/j.jhazmat.2020.124924.
(38) Ying, S. C.; Schaefer, M. V.; Cock-Esteb, A.; Li, J.; Fendorf, S. Depth stratification leads to distinct zones of manganese and arsenic contaminated groundwater. *Environ. Sci. Technol.* **2017**, *51* (16), 8926−8932.
(39) Mozumder, M.; Michael, H.; Mihajlov, I.; Khan, M.; Knappett, P.; Bostick, B.; Mailloux, B.; Ahmed, K.; Choudhury, I.; Koffman, T. J. W. R. R., Origin of groundwater arsenic in a rural Pleistocene aquifer in Bangladesh depressurized by distal municipal pumping. *Water Resour. Res.* 2020, *56* (7), e2020WR027178, DOI: 10.1029/2020wr027178.
(40) Stuckey, J. W.; Schaefer, M. V.; Kocar, B. D.; Benner, S. G.; Fendorf, S. J. N. G., Arsenic release metabolically limited to permanently water-saturated soil in Mekong Delta. *Nat. Geosci.* 2016, *9* (1), 70−76, DOI: 10.1038/ngeo2589.
(41) Jönsson, J.; Persson, P.; Sjöberg, S.; Lövgren, L. Schwertmannite precipitated from acid mine drainage: phase transformation, sulfate release and surface properties. *Appl. Geochem.* **2005**, *20* (1), 179.
(42) Chen, M.; Lu, G.; Guo, C.; Yang, C.; Wu, J.; Huang, W.; Yee, N.; Dang, Z. Sulfate migration in a river affected by acid mine drainage from the Dabaoshan mining area, South China. *Chemosphere* **2015**, *119*, 734−743.
(43) Jacobs, J. A.; Lehr, J. H.; Testa, S. M. *Acid mine drainage, rock drainage, and acid sulfate soils: causes, assessment, prediction, prevention, and remediation*; John Wiley & Sons: 2014.
(44) Conley, D. J.; Paerl, H. W.; Howarth, R. W.; Boesch, D. F.; Seitzinger, S. P.; Havens, K. E.; Lancelot, C.; Likens, G. E. Controlling eutrophication: nitrogen and phosphorus. *Science* **2009**, *323* (5917), 1014−1015.
(45) Wurtsbaugh, W. A.; Paerl, H. W.; Dodds, W. K. J. W. I. R. W., Nutrients, eutrophication and harmful algal blooms along the freshwater to marine continuum. *Wiley Interdiscip. Rev.: Water* 2019, *6* (5), e1373, DOI: 10.1002/wat2.1373.
(46) Sherris, A. R.; Baiocchi, M.; Fendorf, S.; Luby, S. P.; Yang, W.; Shaw, G. M. Nitrate in Drinking Water during Pregnancy and

Spontaneous Preterm Birth: A Retrospective Within-Mother Analysis in California. *Environ. Health Perspect.* **2021**, *129* (5), 57001 DOI: 10.1289/EHP8205.
(47) Sposito, G. *The chemistry of soils*; 2nd ed.; Oxford University Press: Oxford, 2008.
(48) Chorover, J.; Brusseau, M. L., Kinetics of Sorption—Desorption. In *Kinetics of Water-Rock Interaction*; Brantley, S. L.; Kubicki, J. D.; White, A. F., Eds.; Springer New York: New York, NY, 2008; pp 109−149.
(49) McBride, M. B. *Environmental chemistry of soils*; Oxford University Press: New York, 1994.
(50) Schaefer, M. V.; Guo, X.; Gan, Y.; Benner, S. G.; Griffin, A. M.; Gorski, C. A.; Wang, Y.; Fendorf, S. Redox controls on arsenic enrichment and release from aquifer sediments in central Yangtze River Basin. *Geochim. Cosmochim. Acta* **2017**, *204*, 104−119.
(51) Cao, X.; Ma, L. Q.; Rhue, D. R.; Appel, C. S. Mechanisms of lead, copper, and zinc retention by phosphate rock. *Environ. Pollut.* **2004**, *131* (3), 435−444.
(52) Jain, A.; Loeppert, R. H. Effect of Competing Anions on the Adsorption of arsenate and arsenite by Ferrihydrite. *J. Environ. Qual.* **2000**, *29*, 1422−1430.
(53) Antelo, J.; Avena, M.; Fiol, S.; López, R.; Arce, F. Effects of pH and ionic strength on the adsorption of phosphate and arsenate at the goethite−water interface. *J. Colloid Interface Sci.* **2005**, *285* (2), 476−486.
(54) Luengo, C.; Brigante, M.; Avena, M. Adsorption kinetics of phosphate and arsenate on goethite. A comparative study. *J. Colloid Interface Sci.* **2007**, *311* (2), 354−360.
(55) Hongshao, Z.; Stanforth, R.; Competitive adsorption of phosphate and arsenate on goethite. *Environ. Sci. Technol.* 2001, *35* (24), 4753−4757, DOI: 10.1021/es010890y.
(56) Gao, Y.; Mucci, A. Individual and competitive adsorption of phosphate and arsenate on goethite in artificial seawater. *Chem. Geol.* **2003**, *199* (1), 91−109.
(57) Neupane, G.; Donahoe, R. J.; Arai, Y. J. C. G., Kinetics of competitive adsorption/desorption of arsenate and phosphate at the ferrihydrite−water interface. *Chem. Geol.* 2014, *368*, 31−38, DOI: 10.1016/j.chemgeo.2013.12.020
(58) Strawn, D. G. J. G. T., Review of interactions between phosphorus and arsenic in soils from four case studies. *Geochem. Trans.* 2018, *19* (1), 10, DOI: 10.1186/s12932-018-0055-6.
(59) Manning, B. A.; Goldberg, S. Modeling Competitive Adsorption of arsenate with Phosphate and Molybdate on Oxide Minerals. *Soil Sci. Soc. Am. J.* **1996**, *60*, 121−131.
(60) Gao, Y.; Mucci, A. Acid base reactions, phosphate and arsenate complexation, and their competitive adsorption at the surface of goethite in 0.7 M NaCl solution. *Geochim. Cosmochim. Acta* **2001**, *65* (14), 2361−2378.
(61) Hartland, A.; Larsen, J. R.; Andersen, M. S.; Baalousha, M.; O'Carroll, D. J. E. S. Association of arsenic and phosphorus with iron nanoparticles between streams and aquifers: implications for arsenic mobility. *Environ. Sci. Technol.* **2015**, *49* (24), 14101−14109.
(62) Carabante, I.; Grahn, M.; Holmgren, A.; Hedlund, J. In situ ATR−FTIR studies on the competitive adsorption of arsenate and phosphate on ferrihydrite. *J. Colloid Interface Sci.* **2010**, *351* (2), 523−531.
(63) Waychunas, G. A.; Rea, B. A.; Fuller, C. C.; Davis, J. A. Surface chemistry of ferrihydrite: Part 1. EXAFS studies of the geometry of coprecipitated and adsorbed arsenate. *Geochim. Cosmochim. Acta* **1993**, *57* (10), 2251−2269.
(64) Harrington, R.; Hausner, D. B.; Bhandari, N.; Strongin, D. R.; Chapman, K. W.; Chupas, P. J.; Middlemiss, D. S.; Grey, C. P.; Parise, J. B. Investigation of Surface Structures by Powder Diffraction: A Differential Pair Distribution Function Study on arsenate Sorption on Ferrihydrite. *Inorg. Chem.* **2010**, *49* (1), 325−330.
(65) Wang, X.; Li, W.; Harrington, R.; Liu, F.; Parise, J. B.; Feng, X.; Sparks, D. L. Effect of Ferrihydrite Crystallite Size on Phosphate Adsorption Reactivity. *Environ. Sci. Technol.* **2013**, *47* (18), 10322−10331.
(66) Violante, A.; Pigna, M. Competitive Sorption of arsenate and Phosphate on Different Clay Minerals and Soils. *Soil Sci. Soc. Am. J.* **2002**, *66* (6), 1788−1796.
(67) Abdala, D. B.; Northrup, P. A.; Arai, Y.; Sparks, D. L. Surface loading effects on orthophosphate surface complexation at the goethite/water interface as examined by extended X-ray Absorption Fine Structure (EXAFS) spectroscopy. *J. Colloid Interface Sci.* **2015**, *437*, 297−303.
(68) Sverjensky, D. A.; Fukushi, K. A predictive model (ETLM) for As(III) adsorption and surface speciation on oxides consistent with spectroscopic data. *Geochim. Cosmochim. Acta* **2006**, *70* (15), 3778−3802.
(69) Fukushi, K.; Sverjensky, D. A. A surface complexation model for sulfate and selenate on iron oxides consistent with spectroscopic and theoretical molecular evidence. *Geochim. Cosmochim. Acta* **2007**, *71* (1), 1.
(70) Fukushi, K.; Sverjensky, D. A. A predictive model (ETLM) for arsenate adsorption and surface speciation on oxides consistent with spectroscopic and theoretical molecular evidence. *Geochim. Cosmochim. Acta* **2007**, *71* (15), 3717−3745.
(71) Namayandeh, A.; Borkiewicz, O. J.; Bompoti, N. M.; Chrysochoou, M.; Michel, F. M. oxyanion Surface Complexes Control the Kinetics and Pathway of Ferrihydrite Transformation to goethite and Hematite. *Environ. Sci. Technol.* **2022**, *56* (22), 15672−15684.
(72) Schwertmann, U.; Cornell, R. M. *Iron oxides in the laboratory: preparation and characterization*. 2nd completely rev. and extended ed.; Wiley-VCH: Weinheim, 2000.
(73) Liao, S.; Wang, X.; Yin, H.; Post, J. E.; Yan, Y.; Tan, W.; Huang, Q.; Liu, F.; Feng, X. Effects of Al substitution on local structure and morphology of lepidocrocite and its phosphate adsorption kinetics. *Geochim. Cosmochim. Acta* **2020**, *276*, 109−121.
(74) Hiemstra, T.; Mendez, J. C.; Li, J. Evolution of the reactive surface area of ferrihydrite: time, pH, and temperature dependency of growth by Ostwald ripening. *Environ. Sci.: Nano* **2019**, *6* (3), 820−833.
(75) Yang, X.; Juhas, P.; Farrow, C. L.; Billinge, S. J., xPDFsuite: an end-to-end software solution for high throughput pair distribution function transformation, visualization and analysis. *arXiv: Mater. Sci.* **2014**, 3, DOI: 10.48550/arXiv.1402.3163
(76) Ressler, T. WinXAS: a Program for X-ray Absorption Spectroscopy Data Analysis under MS-Windows. *J. Synchrotron Radiat.* **1998**, *5* (2), 118−122.
(77) Fendorf, S.; Eick, M. J.; Grossl, P.; Sparks, D. L. arsenate and chromate retention mechanisms on goethite. 1. Surface structure. *Environ. Sci. Technol.* **1997**, *31* (2), 315.
(78) Elzinga, E. J.; Sparks, D. L. Phosphate adsorption onto hematite: An in situ ATR-FTIR investigation of the effects of pH and loading level on the mode of phosphate surface complexation. *J. Colloid Interface Sci.* **2007**, *308* (1), 53−70.
(79) Elzinga, E. J.; Kretzschmar, R. In situ ATR-FTIR spectroscopic analysis of the co-adsorption of orthophosphate and Cd(II) onto hematite. *Geochim. Cosmochim. Acta* **2013**, *117*, 53−64.
(80) Loring, J. S.; Sandström, M. H.; Norén, K.; Persson, P. J. C. A. E. J. Rethinking arsenate coordination at the surface of goethite. *Chem. - Eur. J.* **2009**, *15* (20), 5063−5072.
(81) Soldoozy, S.; Trinh, A.; Kubicki, J. D.; Al-Abadleh, H. A. In Situ and Real-Time ATR-FTIR Temperature-Dependent Adsorption Kinetics Coupled with DFT Calculations of Dimethylarsinate and arsenate on Hematite Nanoparticles. *Langmuir* **2020**, *36* (16), 4299−4307.
(82) Mackay, A. In Some aspects of the topochemistry of the iron oxides and hydroxides, In *Reactivity of solids: Proceedings of the fourth international symposium on the reactivity of solids*; 1960; pp 571−583.
(83) Schwertmann, U.; Murad, E. Effect of pH on the formation of goethite and hematite from ferrihydrite. *Clays Clay Miner.* **1983**, *31* (4), 277−284.

(84) Penn, R. L.; Oskam, G.; Strathmann, T. J.; Searson, P. C.; Stone, A. T.; Veblen, D. R. Epitaxial assembly in aged colloids. *J. Phys. Chem. B* **2001**, *105* (11), 2177−2182.
(85) Banfield, J. F.; Welch, S. A.; Zhang, H.; Ebert, T. T.; Penn, R. L. Aggregation-based crystal growth and microstructure development in natural iron oxyhydroxide biomineralization products. *Science* **2000**, *289* (5480), 751−754.
(86) Bilardello, D.; Banerjee, S. K.; Volk, M. W. R.; Soltis, J. A.; Penn, R. L. Simulation of Natural Iron Oxide Alteration in Soil: Conversion of Synthetic Ferrihydrite to Hematite Without Artificial Dopants, Observed With Magnetic Methods. *Geochem., Geophys., Geosyst.* **2020**, *21* (7), No. e2020GC009037.
(87) Jolivet, J.-P.; Chanéac, C.; Tronc, E. J. C. C., Iron oxide chemistry. From molecular clusters to extended solid networks. *Chem. Commun.* 2004, (5), 481−483, DOI: 10.1039/B304532N.
(88) Sassi, M.; Rosso, K. M. Ab Initio Evaluation of Solid-State Transformation Pathways from Ferrihydrite to goethite. *ACS Earth Space Chem.* **2022**, *6* (3), 800−809.
(89) Yuwono, V. M.; Burrows, N. D.; Soltis, J. A.; Do, T. A.; Penn, R. L. J. F. D. Aggregation of ferrihydrite nanoparticles in aqueous systems. *Faraday Discuss.* **2012**, *159* (1), 235−245, DOI: 10.1039/C2FD20115A.
(90) Burrows, N. D.; Hale, C. R. H.; Penn, R. L. Effect of pH on the Kinetics of Crystal Growth by Oriented Aggregation. *Cryst. Growth Des.* **2013**, *13* (8), 3396−3403.
(91) Penn, R. L.; Tanaka, K.; Erbs, J. J. J. O. C. G. Size dependent kinetics of oriented aggregation. *J. Cryst. Growth* **2007**, *309* (1), 97−102.
(92) Burrows, N. D.; Hale, C. R. H.; Penn, R. L. Effect of Ionic Strength on the Kinetics of Crystal Growth by Oriented Aggregation. *Cryst. Growth Des.* **2012**, *12* (10), 4787−4797.
(93) Derjaguin, B. V.; Landau, L. D. Theory of the stability of strongly charged lyophobic sols and of the adhesion of strongly charged particles in solutions of electrolytes. *Prog. Surf. Sci* **1941**, *43*, 30−59, DOI: 10.1016/0079-6816(93)90013-L.
(94) Lumsdon, D. G.; Fraser, A. R.; Russell, J. D.; Livesey, N. T. New infrared band assignments for the arsenate ion adsorbed on synthetic goethite (α-FeOOH). *Eur. J. Soil Sci.* 1984, *35* (3), 381−386, DOI: 10.1111/j.1365-2389.1984.tb00294.x.
(95) Hiemstra, T.; Van Riemsdijk, W. J. J. O. C. Surface structural ion adsorption modeling of competitive binding of oxyanions by metal (hydr) oxides. *J. Colloid Interface Sci.* **1999**, *210* (1), 182−193.
(96) Geelhoed, J. S.; Hiemstra, T.; Van Riemsdijk, W. H. Phosphate and sulfate adsorption on goethite: Single anion and competitive adsorption. *Geochim. Cosmochim. Acta* **1997**, *61* (12), 2389−2396.
(97) Langmuir, D. *Aqueous environmental*; Prentice Hall: 1997.
(98) Harvey, O. R.; Rhue, R. D. Kinetics and energetics of phosphate Sorption in a multi-component Al(III)−Fe(III) hydr-(oxide) sorbent system. *J. Colloid Interface Sci.* **2008**, *322* (2), 384−393.

https://doi.org/10.1021/acsearthspacechem.3c00232
ACS Earth Space Chem. XXXX, XXX, XXX−XXX